Brigham and Women's Hospital
Founding Member, Mass General Brigham

Optimization, fabrication and validation of three-section planar continuum robot for ureteroscopy

Charles DeLorey[1,2], Satoshi Kobayashi[2,4], Fumitaro Masaki[2,3], and Nobuhiko Hata[2]

1. Department of Mechanical Engineering, Boston University, 110 Cummington Mall, Boston, MA 02215
3. Collaborative Innovation Center, Canon Medical Research USA., 210 Broadway, Cambridge, MA 02139, USA
2. National Center for Image Guided Therapy, Department of Radiology,
Brigham and Women's Hospital and Harvard Medical School, 75 Francis Street, Boston, MA 02115, USA
4. Department of Urology, Kyushu University, 3-1-1 Maidashi, Higashi-ku, Fukuoka, Fukuoka 8128582, Japan

Background

Multi-section robot originally developed for bronchoscopy has been found feasible in ureteroscopy [Kobayashi 2023]. However, it is yet to be known if the section length of the multi-section robot can be optimized for ureteroscopy to improve the robot's maneuverability for kidney stone removal. We conducted a preliminary study to optimize the section lengths of the continuum robot to fit the kidney anatomy, like previous work done for lung anatomy [Kato 2020]. With this design optimization we fabricated a proof-of-concept robot and present performance metrics on a patient-derived phantom.

Keywords — Robotic ureteroscope, continuum robot, surgical robot, ureteroscopy, tendon-driven

Aims

Informed by modeling of robot section length for optimizing reachability in the kidney, optimal combination of section lengths were found. The 4:1 scale proof-of-concept planar robotic ureteroscope design was modeled on an existing planar continuum robot [Kato 2015]. To quantify the robot performance, metrics of procedure time and final reached angle for the upper, middle, and lower calyces were measured on a 3:1 scale axial kidney phantom.

Methods

Robot dimensions are reported in Table 1. A constant curvature (CC) model is found in Figure 2; the corresponding base-to-tip transformation based on kinematics in [Rao 2021] is reported in Figure 4. To achieve continuum motion, the robot is comprised of aligned guide rings arranged along stacked springs. Each bendable section was actuated by antagonistic tendon pairs along the length of the robot, actuated by a servo motor (Figure 3a). Control was accomplished using a direct mapping of the servo range of motion (RoM) to a joystick. Linear motion of the robot is achieved manually. Using the kidney phantom, reachability and actuation behavior of the robot were measured for 3 distinct regions in the 3 kidney calyces: lower (L), middle (M), and upper (U) (Figure 1). Procedure is defined as navigating from the kidney entrance (Figure 1d) to the region of interest. The procedure was repeated 5 times for the 3 regions in each calyx. Robot kinematics and performance are measured using OpenCV ArUco markers as well as first-person footage from a chip-on-tip camera (IK-CT2, Toshiba America Information Systems, Inc, Irvine CA) at the robot's distal end (Figure 3b).

Length (mm)	Diameter (mm)	Section length (mm)	Spring outer diameter (mm)	Reachable workspace arc (mm)	Pitching angle (°)
442.5	16	44	7.1	800	160.6

Table 1: Robot dimensions

Quantitative findings

A reachable workspace arc of 800 mm and a pitching angle of 160.6° was found. Final angles achieved to reach target regions range from 7.2° to 301.4°. Average procedure time for the calyces were reported (L: 27.9 s (SD=14.9 s), M: 41.0 s (SD=23.4 s), U: 39.7 s (SD=3.2 s)) and in Figure 5. All calyces of the 3D-printed phantom were reachable in 33.4 s on average (SD= 16.8 s). ANOVA performed on the procedure times of three calyces showed statistically significant difference ($p = 0.005$), as well as on the final angles achieved ($p=0.004$).

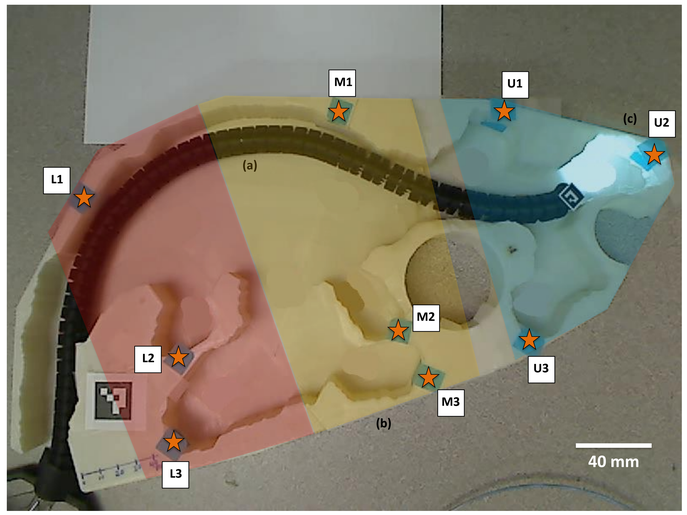

Figure 1: Overhead view of (a) ureteroscope robot in (b) kidney phantom navigating to (c) upper 2nd region. Includes (d) kidney entrance and shaded lower, middle, and upper calyx with labeled target regions (stars)

Achieved procedure times and configurations were similar in target anatomy to those accomplished using a 3D continuum robot endoscope with a different section length configuration on a 3D phantom (Figure 5). Final angles are reported, with the lower calyx showing the most variation (Figure 6, 7). There were no failed procedures.

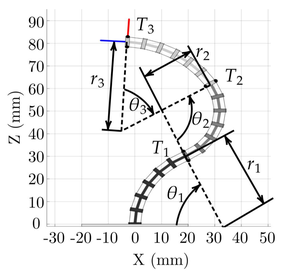

Figure 2: Constant curvature illustration of three-section robot with guide rings [CRVisToolkit, Rao 2021]

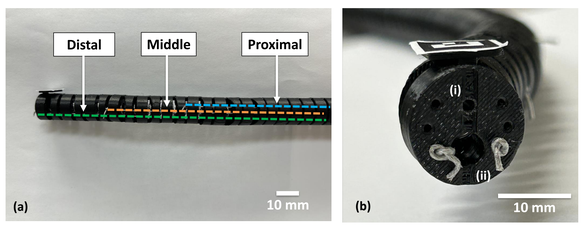

Figure 3: Robot (a) annotated bendable sections with tendons (dotted lines), and (b) robot distal end front view with (i) camera channel and (ii) tool channel

$$\text{(a)}\quad T_i = \begin{bmatrix} cos\theta_i & -sin\theta_i & r_i(1-cos\theta_i) \\ sin\theta_i & cos\theta_i & r_i sin\theta_i) \\ 0 & 0 & 1 \end{bmatrix}, r_i = \frac{1}{\kappa} \qquad \text{(b)}\quad T_F = \prod_{i=1}^{3} T_i$$

Figure 4: Frame transform for (a) *i*th section, and from (b) robot base to tip following CC geometry in Figure 2 (ϕ=0)

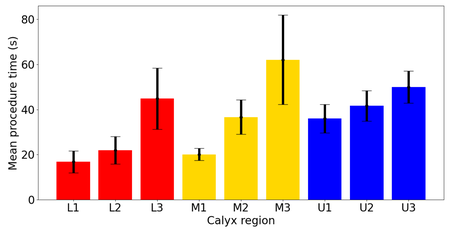

Figure 5: Mean procedure time for all regions

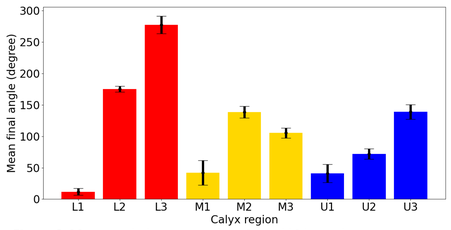

Figure 6: Mean angle between robot tip and kidney phantom entrance at point of region registration for all regions

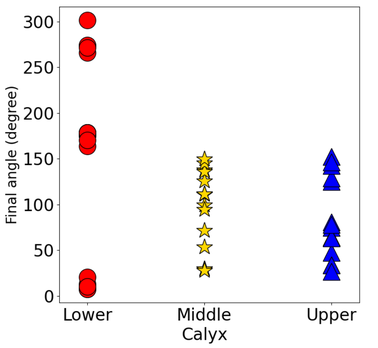

Figure 7: Angle between robot tip and kidney phantom entrance at point of region registration for the three calyces

Conclusion

The performance capabilities of a three-section planar robotic ureteroscope are explored in a kidney phantom. The data suggests a three-section robotic ureteroscope of equal bending section lengths is feasible for navigating kidney regions. Understanding the large anatomical variation found in the kidney, a suitably dexterous and robust robotic ureteroscope can be developed. Additionally, the relatively simple robot design can be utilized to interrogate other research interests and address kinematic restrictions such as RoM and hysteresis. This work informs further development of multi-section robotic ureteroscopes.

References

[1] S. Kobayashi, F. Masaki, F. King, D. Wollin, A. Kibel, and N. Hata, "Feasibility of multi-section continuum robotic ureteroscope in the kidney," Journal of Robotic Surgery, Jan 2023.
[2] T. Kato, F. King, K. Takagi and N. Hata, "Robotized Catheter With Enhanced Distal Targeting for Peripheral Pulmonary Biopsy," in IEEE/ASME Transactions on Mechatronics, vol. 26, no. 5, pp. 2451-2461, Oct. 2021, doi: 10.1109/TMECH.2020.3040314.
[3] T. Kato, I. Okumura, S.E. Song, AJ. Golby, and N. Hata, "Tendon-Driven Continuum Robot for Endoscopic Surgery: Preclinical Development and Validation of a Tension Propagation Model," IEEE ASME Trans Mechatron., 2015 Oct; 20(5):2252-2263.
[4] P. Rao, Q. Peyron, S. Lilge, J. Burgner-Kahrs, "How to Model Tendon-Driven Continuum Robots and Benchmark Modelling Performance," Front Robot AI. 2021 Feb 2;7:630245. doi: 10.3389/frobt.2020.630245. PMID: 33604355; PMCID: PMC7885639.

HARVARD MEDICAL SCHOOL
TEACHING HOSPITAL